# Local detection of X-ray spectroscopies with an in-situ AFM

Mario Rodrigues, Olivier Dhez, Simon Le Denmat, Joël Chevrier, Roberto Felici, Fabio Comin

# Local detection of X-ray spectroscopies with an in-situ AFM

M. S. Rodrigues[1], O. Dhez[1], S. Le Denmat[1], J. Chevrier[2], R. Felici[1] and F. Comin[1]

[1] European Synchrotron Radiation Facility, Grenoble, France

[2] Institut Nel, Grenoble, France

June 3, 2008

## Abstract

We show how the in situ combination of Scanning Probe Microscopies (SPM) with X-ray microbeams enables many new experiments in the synchrotron radiation domain. Our instrument is based on an optics free AFM/STM that can be directly installed on most of the SR X-ray end stations. The instrument can be simply used for AFM imaging of the investigated sample or it can be used for detection of photoemitted electrons with a sharp STM like tungsten tip, thus leading to locally measure the EXAFS signal. Alternatively one can measure the photons absorbed by the tip, thus locally detecting diffraction. In this paper, we show examples of both measurements. We also describe the experimental setup and the tip-beam interaction that is a key point for alignment procedures. We finally show how these features can be exploited in an extended variety of domains, nanosciences and nanomechanics, just to name a few.

## 1 Introduction

SPM techniques are used in many scientific fields ranging from biology to materials sciences. Nowadays, they are thought to be at the hearth of nanosciences. They are easy to use, produce high resolution images of the sample and can unveil many local properties of the surface. Synchrotron Radiation is used instead to probe the atomic and electronic structures of the surfaces averaging on the illuminated area. In the most recent years the importance of X-ray micro and nano beams is steadily increasing and the application of many SPM or SR techniques is often necessary to give a full insight on the sample properties. In micro-nano characterization it is evident the trend to work on a single object whose size can vary from the micro to the nanoscale.

It is then highly desirable to be able to perform SPM and X-ray experiments on the same single object in the same conditions and at the same time. In other words, the combination of both experimental techniques seems to be the first step in a more comprehensive exploration of the micro-nano world. Essentially, two paths have been explored so far. A first one consists in building a UHV SPM chamber that can be installed on a dedicated X-ray beam line (Saito, et al. 2006). The combination of STM and X-rays was aimed here to provide chemical contrast in near field microscopies. 20 nm lateral resolutions have been demonstrated with this technique. The second path is the one we have chosen at the ESRF in the framework of the X-Tip European Project[1]: we considered that an extensive integration of SPM techniques on SR instrumentation could be done only leaving the beamlines as they are, and try to adapt a compact, optic free, AFM/STM on an end station to perform indifferently diffraction or spectroscopy experiments.

Clearly, the aim here is to emphasize versatility, ease of use and the largest possible spectrum of applications. Difficulties are essentially on issues of SPM stability and on the procedures for the simultaneous alignment of the tip, the sample and the microbeams. Piezoelectric detection of the tip-surface interaction based on a quartz tuning fork [TF] has been preferred to avoid repeated optical alignment and difficulties in SPM integration. This becomes a weaker argument as motorized optical fibers can be used to produce state of the art in AFM signal detection and in tip-surface mechanical interaction control. This opens the way to integrate on X-ray diffractometers highly sensitive AFM based on soft levers.

A major difficulty which limits the use of this combination is not the environment that can be vacuum, liquid or gases, but the use of sharp metallic tips. In STM, the tip-surface distance is controlled via the tunneling current: $I(z) = G_o V exp(-z/z_o)$. The value $z_0$ is so small that true atomic resolution can be obtained even with a poor tip. At variance, AFM modes are most often limited by the size of the tip apex, that can be about 10 nm, even though, atomic resolution has been demonstrated using UHV nc-AFM (Giessibl, J. F. 1995). In our instrument these mechanisms cannot be invoked to limit the collection to those electrons or photons emitted by a nm scale surface area. To the contrary, very large areas

[1]STRP 505634-1 X-tip $1^{st}$ March 2004 - 28 February 2007

can probed if no care is taken. In this paper, we shall discuss this problem for each example presented. Surface resolution down to the nanoscale can be achieved by covering the tip with an insulator layer that prevents electrons exchange between the tip and the environment except in the vicinity of the apex. This important issue will be the focus of a forthcoming paper. We shall also describe the X-ray beam interaction with the tip in detail, due to its importance in the alignment and because it is a good candidate for a test sample.

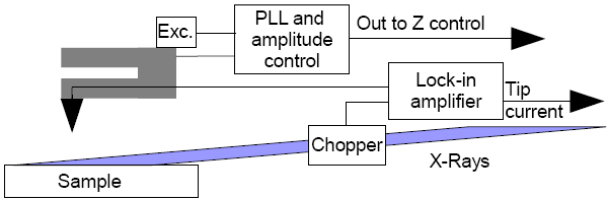


Figure 1: Experimental setup for combination of AFM with X-rays.

## 2 Experimental Set up

The AFM is home made and developed around a quartz tuning fork (TF). Use of tuning forks in SPM design has been the subject of vast literature since TFs are often used in SNOM setups (Karrai, K. et al. 1995). Our instrument operates very much like a conventional AFM but with a simplified set up: unlike conventional AFMs, where the deflection of a cantilever is detected with laser light, AFMs based on TFs have the extra simplicity that the motion of the oscillator is detected directly from conversion of the alternating stress field inside the quartz piezoelectric material into charge. Neither a laser nor a photodetector is needed for the operation of this type of AFMs. This fact simplifies and makes this type of AFMs more robust. However, they may be slower because they must have very high quality factors (Q $\approx$ 8000 while for a conventional cantilever Q $\approx$ 30). In other words, they intrinsically show a very large time constant (t $\approx$ 1s) which actually compensates their rigidity k $\approx$ 20 kN/m (for a conventional cantilever this value is about 40 N/m). The sensitivity very much depends on k/Q and this is roughly the same for a conventional AFM Si cantilever or a TF.

The high Q factor of the TF has led us to choose PLL (Phase Locked Loop) detection to minimize the time needed to obtain an image. In few words, the PLL helps the TF to be close to equilibrium at all times since a feedback loop actively excites the TF at varying frequencies maintaining the phase constant at -90 Deg and thus keeping it at its resonance frequency. TFs can be operated both in shear force mode (Karrai. K, 1995), or in the more conventional, tapping mode. A tungsten tip is glued on the tuning fork by means of a conductive glue to ensure the tip is in electrical contact with the TF electrode connected to the preamp. Assembling a sharp tungsten tip onto an electrically connected TF has become a current procedure in our lab, making SR experiments quite straightforward from this point of view.

The sample is illuminated with time modulated monochromatic X-ray light. A slotted rotating wheel (chopper) is used to modulate the intensity of the beam. The corresponding current detected with the tip is demodulated with a lock-in amplifier. The experimental arrangement is shown in fig. 1. The X-ray beam used to obtain the results presented here was about 4×4 $\mu$m$^2$ with $10^{12}$ photons per second in about $10^{-4}$ bandpass.

The sample consisted of Ge islands of about 1$\mu$m large and 500nm height on an Si matrix. An in-situ AFM image reveals its topography (figure 3).

## 3 Microbeam interaction with the W tip

The first step of the experiment is the alignment of the beam with the tip of the AFM. This is easily done because once the beam illuminates the tip, due to photoelectric effect, a cascade of electrons will flow out of the tip. This produces a measurable current which is the signal we record. This current has been systematically recorded as the tip is moved in the XZ plane, perpendicular to the incidence of the beam. This produces experimental images of the tip shown in fig. 2 (a) and the respective profiles in fig. 2 (c).

A characteristic feature when the tip is scanned by the X-ray beam is an enhanced current when the X-ray beam is at grazing incidence on the tip. This produces the higher contrast surrounding the tip and is visible in fig. 2a and 2b. This is the point we want to explain in some detail as it is the key result to understand the interaction of the X-ray beam with the tip.

The relevant parameters to analyze the experimental results of figure 2a are the linear absorption coefficient $\mu_l$, which is of few microns for the energy considered here, the inelastic mean free path $\lambda$ for $e^-$ in solids, which is typically of few $\AA$ (Tanuma et. al., 1991 ), and the characteristic energy lost per unit of length i.e. the stopping power S(E) for electrons (Ashley, J. C. et al. 1976).

After creation, electrons undergo inelastic scattering processes and loose their energy throughout their path very fast. This, associated with a very small value of $\lambda$, leads to an escape depth $d_{eff}$ in the order of tenths of nm.

The probed depth as well as the amount of current

Figure 2: a) Current flowing from the W tip as a function of its position relative to the X-ray beam. b) Simulation of a). c) cross sections of a) and b). d) current from the tip as a function of photon energy across the$L_3$ edge of the W tip.

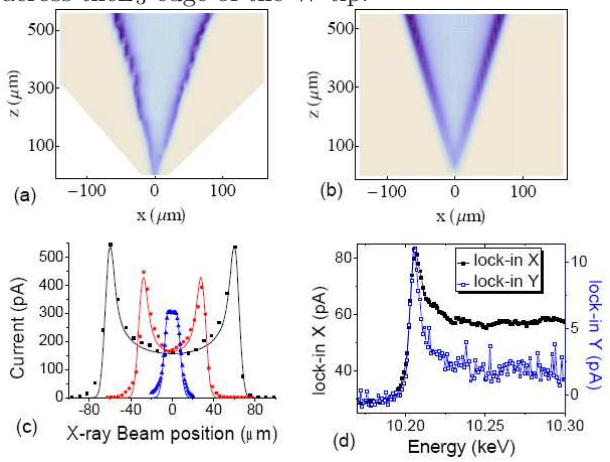


emitted from an illuminated surface depend on $d_{eff}$.

In order to quantify the results, we define the effective escape depth $d_{eff}$ as the depth that has a probability $\pi/12$ that a photon absorbed at a distance smaller than $d_{eff}$ will result in one electron escaping the tip. The other $e^-$ go further into the tip and do not escape. The factor $\pi/12$ corresponds to the 1/2 of the volume of a sphere with radius 0.5 which is the escape probability for an $e^-$ created at a distance $d_{eff}$ and taking the shortest path to the surface. This factor takes into account all possible paths for the $e^-$.

Considering the complexity of the photon absorption processes, their conversion into electrons, and how these electrons are loosing their kinetic energy, it is clear that such a definition is oversimplified. However, it is sufficient to take in account the measurements and provide a reasonable analysis.

We then calculated the intensity of the current $i(x,z)$. We have taken into account the 2D Gaussian beam shape and the linear absorption length on W for photons of 10 keV ($\mu = 5.8$ $\mu$m). The current is given by:

$$i(x,z) = \int\int I(x,z)\frac{\pi}{12}f(x,z)(1-e^{-t(x,z)/\mu_l})dxdz \quad (1)$$

$I(x,z)$ is the Gaussian distribution of the photons, $f(x,z)$ takes into account only the number of photons that are absorbed in the tip close enough to its surface and $t(x,z)$ is the length along which the absorbed photons produce measurable current. Both $f(x,z)$ and $t(x,z)$ depend on the geometry of the tip as well as on the geometry of the incidence and therefore both depend on the parameter $d_{eff}$. If the radius of the tip is smaller than $d_{eff}$ then $f = 1$ and $t(x,z)$ is simply the thickness $t = \sqrt{R(z)^2 - x^2}$ with $R(z)$ the radius of the tip at position $z$. If the radius of the tip is larger than $d_{eff}$ and the beam is incident on the tip perpendicular to it, then $t(x,z) = d_{eff}$.

On the basis of this calculation we can now estimate $d_{eff}$. Figure 2a, 2b and 2c show the agreement between measured current versus the tip position relative to the beam. The only adjustable parameter is $d_{eff}$. All other quantities are estimated from experimental conditions. From our experiments, we systematically obtain $d_{eff}$ of about 30 nm.

We can try to relate $d_{eff}$ to the stopping power of W, or better, to the CSDA (Continuous Slowing Down Approximation) range which according to NIST Physical Reference Data (ESTAR database)[2] is one order of magnitude higher.

The only source of error while computing $d_{eff}$ is the flux, since the total current can be approximated by $i = eI_0 \times d/\mu$, provided $d << \mu$, as can be concluded from equation 1. Although the flux is only approximately given it is not enough to account for the discrepancy.

It is worth mentioning that the W surface of the tip is not treated before the experiments. There is always a native oxide which increases the work function of W therefore decreasing the TEY (Total Electron Yield). This could explain at least part of the difference between expected and experimentally determined $d_{eff}$.

As a final remark, we would like to point out that additional information on the TEY is coming from the use of a lock-in in detecting the signal. In figure 2 (d) as we scan around the $L_3$ edge of tungsten, we see the edge jump both in the lock-in signals X and Y. X is in phase with the signal, while Y is out of phase yielding a value close to zero along all the scan except at the white line. We propose this is caused by the fluorescence yield as there is a substantial amount of photons that can go out of the tip, ionize the air surroundings and create a current which is not in phase with the primary current.

# 4 XAS and AFM

The goal here is to select an individual particle or a specific region of the sample to be studied and measure XAS (X-ray absorption spectroscopy) signal with the tip.

The following experimental procedure has been applied to locate the Ge islands below the tip.

If we park the tip few $\mu$m above the sample and move the whole AFM (no relative motion between the tip and the sample) upwards relative to the beam, we first measure a signal due to beam on tip (region I fig.

[2] http://physics.nist.gov/PhysRefData/Star/Text/contents.html

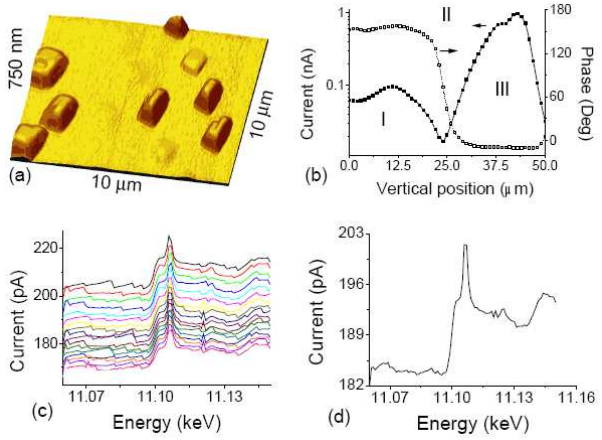


Figure 3: (a) In-situ AFM image; (b) beam incident on the W tip (I), beam passing the tip and the sample (II), beam illuminating sample (III); (c) Several measures of the Ge edge; (d) average of (c)

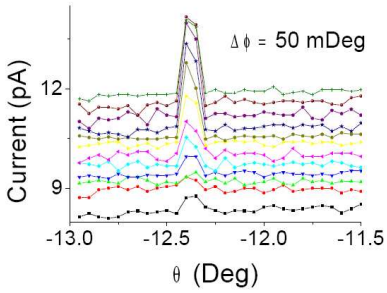


Figure 4: photocurrent from the W tip as a function of the incidence angle $\theta$, and azimuthal $\phi$

3b). As we further lift the AFM, we observe a minimum corresponding to the position where the beam is passing between the tip and the sample (region II on fig. 3b). Moving even more the AFM upwards relative to the beam, we end up illuminating the region of the sample below the tip resulting in a maximum (region III on fig. 3b) of signal from the illuminated sample. The phase of this signal shifts $\pi$ indicating a reversal in the current direction.

This is because when the beam illuminates the tip a cascade of electrons flow out of it, while when it illuminates the sample a cascade impinges on it.

When we measured the AFM image shown in figure 3a, we were expecting to measure a contrast in the current as the tip goes through the isolated islands. The fact that this contrast could not be seen tells us that, with regular STM tips, the lateral resolution is dominated by the footprint of the beam. In our particular case, the beam illuminated 8 to 12 of these islands, which corresponds to an area slightly bigger than that of image 3a.

In this configuration, with the tip located 10 $\mu$m above the surface, we can analyze the current variation issued from this area as the beam energy is varied across the Ge K edge. This result is presented in figure 3c and 3d where we plot the current flowing from the tip as a function of the energy.

From the data, we conclude that the Ge islands were quite oxidized. This is indicated by the presence of a shoulder before the white line, (Greegor R. B. et. al. 1987). This is an important piece of information that could not be obtained with the AFM alone.

On the other hand, if XAS had been taken in a conventional form, the topography of the illuminated sample would not have been revealed.

With the current trend towards SR "nanobeams" it will be harder and harder to tell which part of the sample is being investigated.

It is our believing that the techniques described here will have an important impact in this context.

To limit the area from which electrons are collected, we are developing new "smarter" tips, which are STM tips isolated down to the apex with only a very small opening at the extremity.

This will be similar to what other groups have done, see for example (Akiyama, K. et al. 2005), where tips have been covered with glass to decrease the background. In our case, we want to do more than just decrease the background, we want to laterally confine the measurement. Doing so, we hope to achieve a lateral resolution of about 30 nm. For the high fluxes we have at the ESRF, this confinement will still result in appreciable current flowing to the tip.

# 5 Diffraction and AFM

We now want to show that Bragg reflections can be measured through collection of photons by the tip. The tip was parked few $\mu$m above the sample. The angle of incidence of the beam was then scanned. The germanium Bragg condition was set for the (3 1 1) at 12 Deg for a monochromatic beam with energy close to the K edge of Ge.

The peak was detected with the AFM tip and is shown in figure 4 for different azimuthal $\phi$.

The crystallographic alignment of the Ge islands have been done exclusively using the tip as a detector.

Diffraction is usually measured with a detector set at $2\theta$ far away from the sample. Typically the detector is located about one meter after the sample and collects photons in a very small solid angle, thus giving a very high angular resolution in the detection. The use of a STM tip to detect the diffracted photons cannot give the same angular resolution, but instead, can give a very high spatial resolution capable of re-

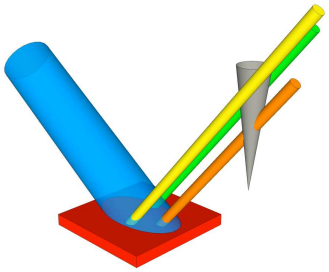

Figure 5: schematic illustration describing how the diffracted X-ray beam can impinge on the AFM tip, resulting in figure 3b.

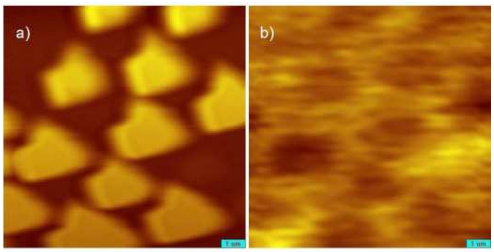


Figure 6: (a) AFM image; (b) current image: the contrast in the current image in which we see the Ge islands as holes, is because the tip collects the diffracted x-rays which subtracts from the photoelectrons

solving beams diffracted from different nanoareas as illustrated in figure 5.

As an example, we show the results obtained using the tip as a photon detector while acquiring simultaneously an AFM image. When in Bragg conditions the current signal shows a significant contrast as shown in figure 6, that disappears completely when the sample is not in Bragg condition. From the contrast in figure 6b we can identify each of the islands shown in image 6a.

The particles are seen as holes, since the diffracted photons impinging on the W tip extract electrons away, which causes a decrease in the overall current which is mainly due to the electrons photoemitted from the sample.

The AFM image suffers of a great tip effect. The sample is the same as in figure 3 and the islands should resemble more those of that figure. The deformation is due to the fact that the tip was used for quite a while and became blunt.

Here again, the contrast we observe in the tip current as the tip cuts through the array of diffracting beams will be enhanced if we isolate the tips except at the apex, since this will prevent photo-electrons generated in the tip, far from its apex, to escape away. Moreover, smart tips will provide more angular resolution in the scattering plane. Furthermore, the background (see figure 4) due to emitted charges from the sample and or from air will almost disappear, strongly enhancing then the detection of photons.

We are at the moment developing tips and techniques which will allow us to collect photoelectrons and photons only with the apex of the tip. This will increase the lateral and angular resolution of our experiments as well as decrease the background.

Finally, it will be possible to obtain a XAS contrast or diffraction data while simultaneously acquiring an AFM topographical image.

In a different experiment, we are also trying, with other groups, to measure diffraction from an individual nano crystal while the AFM tip mechanically interacts with it.

We thank D. Wermeille from ID3 ESRF for his help at the beam line. We thank T. H. Metzger, C. Mocuta and K. Mundboth from ID1 at ESRF for discussions. This work was supported by the E.U. FP6 program, under contract STRP 505634-1 X-tip.

Akiyama, K., Eguchi, T., An, T., Hasegawa, Y., Okuda, T., Harasawa, A., Kinoshita, T., (2005) *Review of Scientific Instruments* **76** 083711-3

Giessibl, F. J. (1995) *Science* **267** 68-71

Greegor, R. B., Lytle, F. W., Kortright, J., Fischer-Colbrie, A. (1987) *Journal of Non-Crystalline* **87** 311-325

J.C. Ashley, C. J. Tung, R. H. Ritchie, and V. E. Anderson. (1976) *IEEE Trans. Nucl. Sci.* **NS-23** 1833-1840

J.K. Gimzewski, R. Berndt and R.R. Schlittler, (1992). *Ultramicroscopy* **366-37**, 42-44

Karrai, K., and Grober, R. D. (1995). *Appl. Phys. Lett.* **66**, 1842-1844

Karrai, K., and Grober, R. D., (1995), *Ultramicroscopy* **61** 197-205

Saito, A., Maruyama, A., Manabe, K., Kitamoto, K., Takahashi, K.,Takami, K., Yabashi, M., Tanaka, T., Miwa, D., Ishii, M., Takagi, Y., Akai-Kasaya, M., Shin, S., Ishikawa, T., Kuwaharaa, Y., Aonoa, M.. (2006). *Journal of Synchrotron Radiation* **13**, 216-220.

Tanuma, S., Powel, D. J. and Penn., D. R. (1991), *Surf. Interface. Anal.* **17** 927-931